JACS
JOURNAL OF THE AMERICAN CHEMICAL SOCIETY

Article

pubs.acs.org/JACS

# A Detailed Study of the Magnetism of Chiral {$Cr_7M$} Rings: An Investigation into Parametrization and Transferability of Parameters

Elena Garlatti,[†] Morten A. Albring,[‡] Michael L. Baker,[‡,§] Rebecca J. Docherty,[‡] Hannu Mutka,[§] Tatiana Guidi,[∥] Victoria Garcia Sakai,[∥] George F. S. Whitehead,[‡] Robin G. Pritchard,[‡] Grigore A. Timco,[‡] Floriana Tuna,[‡] Giuseppe Amoretti,[†] Stefano Carretta,[†] Paolo Santini,[†] Giulia Lorusso,[⊥,¶] Marco Affronte,[⊥] Eric J. L. McInnes,[‡] David Collison,[‡] and Richard E. P. Winpenny*[,‡]

[†]Dipartimento di Fisica e Scienze della Terra, Università di Parma, via G.P. Usberti 7/a, 43123 Parma, Italy

[‡]School of Chemistry and Photon Science Institute, University of Manchester, Oxford Road, Manchester M13 9PL, United Kingdom

[§]Institut Laue-Langevin, BP 156, 6 rue Jules Horowitz, 38042 Grenoble Cedex 9, France

[∥]ISIS Facility, Rutherford Appleton Laboratory, Didcot OX11 0QX, United Kingdom

[⊥]Dipartimento di Fisica, Università di Modena e Reggio Emilia, via Campi 213/a, 41100 Modena, Italy

Supporting Information

**ABSTRACT:** Compounds of general formula $[Cr_7MF_3(Etglu)(O_2C^tBu)_{15}(Phpy)]$ [$H_5Etglu$ = *N*-ethyl-D-glucamine; Phpy = 4-phenylpyridine; M = Zn (**1**), Mn (**2**), Ni (**3**)] have been prepared. The structures contain an irregular octagon of metal sites formed around the pentadeprotonated $Etglu^{5-}$ ligand; the chirality of *N*-ethyl-D-glucamine is retained in the final product. The seven $Cr^{III}$ sites have a range of coordination environments, and the divalent metal site is crystallographically identified and has a Phpy ligand attached to it. By using complementary experimental techniques, including magnetization and specific heat measurements, inelastic neutron scattering, and electron paramagnetic resonance spectroscopy, we have investigated the magnetic features of this family of {$Cr_7M$} rings. Microscopic parameters of the spin Hamiltonian have been determined as a result of best fits of the different experimental data, allowing a direct comparison with corresponding parameters found in the parent compounds. We examine whether these parameters can be transferred between compounds and compare them with those of an earlier family of heterometallic rings.

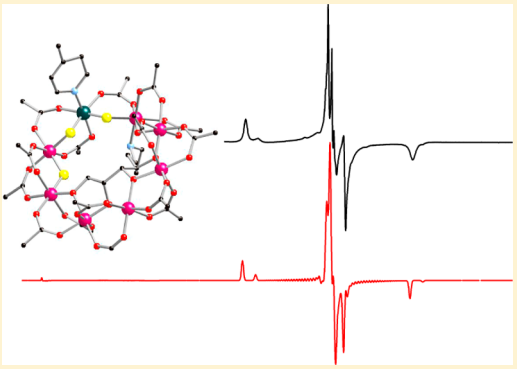

## INTRODUCTION

Fitting observed data to a model is one of the most fundamental actions in science. The aim should always be to use the simplest possible model that fits all of the observations. Molecular magnetism is an area that produces beautiful noninteracting quantum objects that allow us to test such models.[1] This has led to studies of quantum phenomena such as tunneling of magnetization[2] and direct evidence for the Berry phase in a magnetic object.[3] Compounds containing a ring of metal ions have been heavily studied; one of the first very high spin molecules was the {$Mn_6$} ring reported by Gatteschi and Rey,[4] and the study of a "ferric" wheel prepared by Lippard's group[5] has been very influential, involving the observation of clear steps in magnetization measurements and the proposal that the system could be interpreted using spin waves.[5] Later work has included studies of tunneling of the Néel vector.[6] Our own work on homometallic rings of spin centers has recently allowed the direct demonstration of spin dynamics in a molecular magnet[7] using inelastic neutron scattering (INS) without the need for a spin Hamiltonian, and we have described detailed studies of a nine-metal ring that shows spin frustration.[8]

We have also studied in great detail heterometallic rings in which one divalent metal is included in an array of trivalent metals.[9] In the first family of such rings, which are green in color and of general formula $[NH_2R_2][Cr_7MF_8(O_2C^tBu)_{16}]$ (R = a linear alkyl, typically ethyl; M = a divalent ion, e.g., $Ni^{II}$, $Mn^{II}$, $Zn^{II}$, $Co^{II}$, $Cu^{II}$), a regular octagon of metal sites is found with the divalent metal site largely disordered about the eight sites of the octagon. Each edge is bridged by one fluoride and two pivalates, and we have found crystallographic symmetry as high as $D_{4d}$. Our studies of such systems have involved the observation of tunneling of the total spin of a molecular magnet,[10] including a direct measurement of the tunnel gaps at avoided crossings by INS.[11] We also reported the first measurements of coherence times on molecular nanomagnets.[12] We have proposed that such molecules could be used as

**Received:** May 14, 2014
**Published:** June 26, 2014





dx.doi.org/10.1021/ja5047445 | *J. Am. Chem. Soc.* 2014, 136, 9763−9772

qubits within quantum information processing[13] and have demonstrated that we can link two such molecules.[14] Recently we have shown we can coherently manipulate the electron spins in crystalline samples of such magnetic rings.[15]

This family of green {$Cr_7M$} rings gives remarkably beautiful spectra in both INS and electron paramagnetic resonance (EPR) spectroscopy, which has allowed us to characterize them very precisely.[9] The thermodynamic and spectroscopic properties of these heterometallic rings can be modeled using two isotropic exchange interactions ($J_{CrCr}$ and $J_{CrM}$) and two sets of single ion parameters (i.e., $d_{Cr}$ and $d_M$, where $d$ is the axial zero-field splitting parameter). To model EPR spectra for these rings, anisotropic exchange parameters were introduced.[16]

Understanding of the low-temperature physics of molecular nanomagnets invariably involves the use of a range of experimental techniques and normally a mathematical description based on a spin Hamiltonian. Such models are dependent on the symmetry and nuclearity of the system studied. Early work in molecular magnetism often focused on dimetallic complexes where only one parameter—the isotropic exchange interaction, $J$—was significant in the spin Hamiltonian. As larger, less symmetric structures have been studied, more exciting physics has been discovered, and the number of parameters needed in the spin Hamiltonian has increased. This brings us to the general problem of choosing a mathematical model that is as simple as possible but matches all of the observations. First, the molecular magnet will have been characterized by X-ray crystallography, giving a molecular structure that might contain multiple metal centers that are not identical by symmetry, which could lead to multiple exchange paths and multiple unique coordination environments for individual ions. A structure can often justify many more spin Hamiltonian parameters than are needed to fit the magnetic and spectroscopic data. Second, where there are many parameters there is a much greater chance of correlation between parameters when fitting. Third, the computational resources required increase as more and more parameters are introduced. These problems are significant if we wish to understand the low-temperature physics precisely in complicated polymetallic compounds. Here we report an ideal system for studying how models can be developed and the restrictions of such models even where very large amounts of data are available.

Here we discuss a second series of rings, which are purple in solution and the solid state.[17] The formula is [$Cr_7MF_3$(Etglu)-($O_2C^tBu$)$_{15}$(Phpy)] [$H_5$Etglu = *N*-ethyl-D-glucamine; Phpy = 4-phenylpyridine; M = Zn (**1**), Mn (**2**), Ni (**3**)]. $Etglu^{5-}$ is chiral, and this chirality is maintained in the metal rings. These rings have eight different edges and are therefore an excellent test case for examining the transferability of parameters between different molecular nanomagnets. To understand these rings, we have used four distinct experimental techniques providing complementary information: magnetic measurements, heat capacity measurements, INS, and EPR spectroscopy. We then describe these systems with a full microscopic spin Hamiltonian using the same level of description (i.e., the same number of parameters in the same spin Hamiltonian) as used for the green {$Cr_7M$} rings in order to have a direct comparison. The change is from a system with $D_{4d}$ symmetry to one with $C_1$ symmetry.

The first issue we intend to address here is to find a minimum set of parameters that can describe a broad set of experimental data. This is not trivial since different experiments are sensitive to different parameters and we need to converge to only one consistent set. Second, we wish to investigate whether spin Hamiltonian parameters are transferable between similar structures. As compounds **1**−**3** are isostructural, we can examine this for molecules that have an identical atomic structure but different spin-state structures. We proceed as follows: High-temperature susceptibility and magnetization data are used to assess the isotropic exchange interactions ($J$) and the $g$ values, while low-temperature specific heat data are sensitive to the zero-field splitting of the lowest multiplets and fix the energy scale of the magnetic anisotropy. INS data are then used to confirm these parameters and generate an energy spectrum for the low-lying energy states of the system. Finally EPR spectroscopy is used to interrogate the anisotropy of the lowest-lying states. We conclude by comparing these results with parameters obtained for other Cr-based rings. This systematic study and comparison of two families of rings provides a test of ideas such as transferability of parameters between different magnetic molecules.

## RESULTS AND ANALYSIS

**Synthesis.** Simple secondary amines have previously been used as a template about which to grow octagonal {$Cr_7Ni$} rings.[9] If we use *N*-ethyl-D-glucamine ($H_5$Etglu, $C_8H_{14}NO_5H_5$) as a secondary amine, the polyol becomes deprotonated and the polyalkoxide acts as a bridging ligand. The reaction produces [$Cr_7MF_3$(Etglu)($O_2C^tBu$)$_{15}$($H_2O$)] in yields of 38% for M = Zn (**1**), 42% for M = Mn (**2**), and 43% for M = Ni (**3**). In a second step, which is essentially stoichiometric, 4-phenylpyridine replaces the water by a simple substitution reaction to produce a molecule that is more stable for physical studies. Full details are given in the Supporting Information. Use of polyols in cluster synthesis goes back to work on metallomacrocycles from Saalfrank[18] and has recently been pursued by a number of groups.[19] *N*-Ethyl-D-glucamine does not appear to have been used as a ligand prior to this work.

**Structural Considerations.** Compounds **1**, **2**, and **3** are isostructural and contain eight metals arranged at the corners of an irregular octagon (Figure 1). The internal edges of the octagon are bridged by three fluorides and five alkoxides derived from $Etglu^{5-}$. The divalent site is ordered and bound to two bridging fluorides, three bridging pivalate ligands, and a terminal phenylpyridine ligand. The seven $Cr^{III}$ sites have four distinct coordination environments. One site adjacent to the divalent site (Cr7) has an N-donor from $Etglu^{5-}$ coordinated to it, one bridging fluoride, one bridging alkoxide, and three bridging pivalates. The other site adjacent to the $M^{II}$ site (Cr1) is bound to two bridging fluorides and four oxygens from pivalates. The Cr2 site is bound to a single bridging fluoride, a single bridging alkoxide, and four pivalates, while the remaining four $Cr^{III}$ sites are bound to two bridging alkoxides and four pivalates. Five Cr···Cr edges of the ring are bridged by a single alkoxide and two pivalates, and the Cr1−Cr2 edge is bridged by a single fluoride and two pivalates; the two Cr···M edges vary, with one bridged by one fluoride and one pivalate and the second bridged by one fluoride and two pivalates. The chirality of the molecule means that the $C_1$ symmetry of the ring is retained in all states, and thus we need not worry about a change in symmetry between measurements.

The octagon is therefore irregular. In all three structures, the five alkoxide-bridged Cr···Cr contacts fall in the range 3.32−3.40 Å. The two edges bridged by a fluoride and two pivalates fall in the range 3.40−3.44 Å. The Cr−M edge bridged by one


dx.doi.org/10.1021/ja5047445 | J. Am. Chem. Soc. 2014, 136, 9763−9772

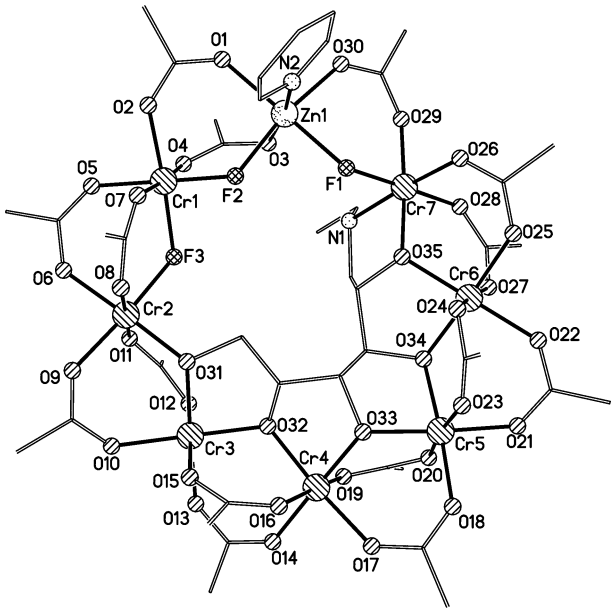


**Figure 1.** Structure of $[Cr_7ZnF_3(Etglu)(O_2C^tBu)_{15}(Phpy)]$ (**1**) in the crystal. The methyl groups of pivalates, the phenyl group, and all of the H atoms have been excluded for clarity.

fluoride and one pivalate is longer in every case, falling in the range 3.55−3.58 Å. Most of the M···M···M angles within the octagon are close to that expected for a regular octagon (135°); the two exceptions are the Cr1−M1−Cr7 angle, which is near 120° in each structure, and the Cr4−Cr5−Cr6 angle, which is around 127° in all of the compounds. The octametallic ring is not planar, with a mean deviation from planarity of near 0.3 Å. In each structure, Cr7 is the metal ion furthest (0.7 Å) out of the mean plane defined by the distorted octagon. The lack of planarity is presumably caused by the involvement of the templating $Etglu^{5-}$ group.

The bond lengths show the expected trends. Full tables of bond lengths and angles are given in the Supporting Information. The bonds to the divalent metal sites fall in the ranges 2.05−2.13 Å for **1** (Zn), 2.03−2.13 Å for **2** (Mn), and 2.00−2.09 Å for **3** (Ni). The bonds to $Cr^{III}$ are generally normal with a few exceptions. The bonds to fluorides bridging to the divalent center (F1 and F2) are shorter than other Cr−X bonds, falling in the range 1.88−1.90 Å. The bonds to the N-donor from $Etglu^{5-}$ are longer, in the range 2.08−2.12 Å. The remaining bonds, to O-donors or F3, average 1.96 ± 0.04 Å.

The bond angles are also normal. To investigate potential superexchange pathways, the bond angles at the bridging fluorides and bridging alkoxides were examined. All of the Cr−O−Cr angles fall in a narrow range from 118 to 122°. The single Cr−F−Cr angle is around 124° in each structure. The two M−F−Cr angles in the structure are quite different: the angle at the fluoride bridging to Cr7 (F1 in Figure 1) is around 131° in all three structures, while the angle at the F bridging to Cr1 (F2 in Figure 1) is around 122° in each case.

The variation in the structural parameters of the three structures is therefore quite small. The Cr···Cr contacts are all quite similar, and there is little change in the Cr−X−Cr bridging angle for fluoride and alkoxide. The two Cr···M contacts within the ring are quite different from one another.

**Theory.** The simulations below use the following microscopic Hamiltonian operator:

$$H = \sum_{i=1}^{8} J_i s_i \cdot s_{i+1} + \sum_{i=1}^{8} s_i \cdot \mathbf{D}_i \cdot s_i + \mu_B \sum_{i=1}^{8} \mathbf{B} \cdot g_i \cdot s_i \quad (1)$$

Sites $i$ = 1 to 7 are occupied by $Cr^{III}$ ions, while site $i$ = 8 is occupied by the divalent metal ion $M^{II}$ (usual cyclic boundary conditions are applied so that $s_9 = s_1$). The first term in eq 1 describes the Heisenberg−Dirac−Van Vleck exchange interaction. We use a minimal model with only two exchange interactions: $J_{CrCr}$ describes the exchange interactions between pairs of $Cr^{III}$ ions and $J_{CrM}$ describes the interaction between a $Cr^{III}$ ion and the $M^{II}$ ion. The second term describes local crystal field (zero-field splitting) interactions, and the $z$ axis is chosen to be perpendicular to the mean plane of the ring. This crystal field interaction can be expressed as a sum of an axial term $d_i$ and a rhombic term $e_i$:

$$\sum_{i=1}^{8} s_i \cdot \mathbf{D}_i \cdot s_i = \sum_{i=1}^{8} d_i \left[ s_{z,i}^2 - \frac{1}{3} s_i(s_i + 1) \right] + \sum_{i=1}^{8} e_i [s_{x,i}^2 - s_{y,i}^2] \quad (2)$$

We chose to include only a single $d_i$ and $e_i$ for all of the $Cr^{III}$ sites and distinct $d_M$ and $e_M$ for the divalent site if it is paramagnetic. This is the minimal possible model for anisotropy, which also effectively takes into account dipolar effects. The third term in 1 is the Zeeman term. Throughout the simulations discussed below, we used $g_{Cr}$ = 1.98 and $g_{Mn}$ = 2.00. For compound **3** we allowed the $\mathbf{g}_{Ni}$ matrix to vary to obtain the best simulations.

Long-range inter-ring interactions are negligible because there are no paths for superexchange and because the inter-ring dipolar interaction is small as a result of the small total spin of the rings at low temperature.

**Magnetic and Heat Capacity Measurements and Inelastic Neutron Scattering.** *Compound 1: $Cr_7Zn$.* As $Zn^{II}$ is diamagnetic, compound **1** is the best starting point because it allows us to determine the $Cr^{III}$ parameters in the Hamiltonian (eq 1). The magnetic susceptibility $\chi$ (Figure 2a)

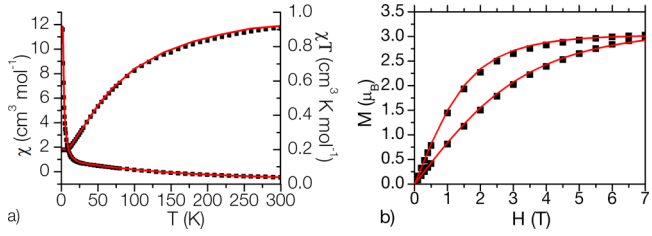


**Figure 2.** (a) Susceptibility $\chi$ and $\chi T$ of **1** measured at 100 mT from 2 to 300 K and (b) DC magnetization ($M$) of **1** measured at 2 and 4 K. The observed data are shown as black squares; red lines are simulations using the parameters in Table 1.

increases slowly with decreasing temperature until approximately 23 K, below which $\chi_m$ rises rapidly. This is evidence of a nonzero spin ground state. $\chi_m T$ falls smoothly with temperature, showing that the predominant interaction between spins is antiferromagnetic, and plateaus at 11.66 $cm^3$ K $mol^{-1}$. The saturation value of the magnetization at 2 K is 3.0 $\mu_B$ (Figure 2b), consistent with a ground spin state $|S = {}^3/_2\rangle$. Simulations of the susceptibility and magnetization were performed using the MAGPACK package.[20] Both curves can be reproduced using a single $J_{CrCr}/k$ value of 20 K (solid red lines in Figure 2; Table 1).


dx.doi.org/10.1021/ja5047445 | J. Am. Chem. Soc. 2014, 136, 9763−9772

**Table 1. Spin Hamiltonian Parameters for Compounds 1−3**

| compound | $J_{CrCr}/k$ (K) | $J_{CrM}/k$ (K) | $d_{Cr}/k$ (K) | $e_{Cr}/k$ (K) | $d_M/k$ (K) | $e_M/k$ (K) |
|---|---|---|---|---|---|---|
| **1** | 20 | – | −0.34 | −0.09 | – | – |
| **2** | 20 | 12 | −0.34 | −0.09 | −0.04 | – |
| **3** | 20 | 30 | −0.34 | −0.09 | −7.3 | 0.75 |

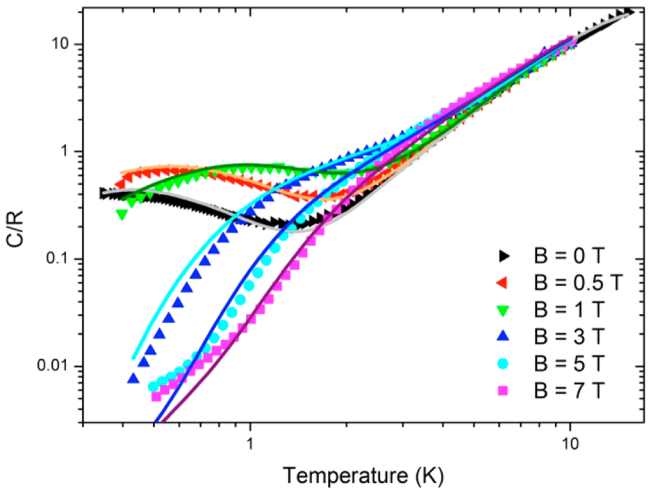


**Figure 3.** Temperature dependence of the specific heat, normalized to the gas constant $R$, for compound **1** in different applied magnetic fields as noted in the inset. Solid lines represent simulations using the parameters reported in Table 1. Colors of solid lines match experimental data except dark blue solid line for 5 T and light blue line 3 T.

The calculation of the specific heat (Figure 3) was performed using the expressions for the lattice contribution $C_{latt}$ (eq 3) and the magnetic contribution $C_m$ (eq 4):[5]

$$\frac{C_{latt}}{R} = \frac{234 r_D T^3}{[\theta_D + \varepsilon T^2]^3} \quad (3)$$

where $r_D$ is the number of atoms per molecule fitting the Debye temperature with $\theta_D$ = 156 K and $\varepsilon$ = 0.4 $K^{-1}$, and

$$\frac{C_m}{R} = \beta^2\{[\sum_i E_i^2 \exp(-\beta E_i)][\sum_i \exp(-\beta E_i)] - [\sum_i E_i \exp(-\beta E_i)]^2\}/[\sum_i \exp(-\beta E_i)]^2 \quad (4)$$

where $\beta = 1/kT$ and the lowest-lying energy levels $E_i$ were obtained by considering the anisotropy terms in addition to the $J_{CrCr}$ exchange interaction in the spin Hamiltonian (eq 1). It should be noted that the curvature of $C(T)$ in zero applied field (Figure 3) clearly shows the Schottky anomaly due to the splitting of the ground spin state $|S = {}^3/_2\rangle$, thus fixing the energy scale of this splitting.

INS spectra provide important information on low-lying spin states and a direct determination of the $J_{CrCr}$ exchange interaction. The high-energy transfer spectra at 1.8, 7, and 20 K clearly show a strong cold transition at 2.3 meV and a hot transition at 1.65 meV (Figure 4a). The high-resolution/low-energy spectrum at 1.8 K also shows a cold transition at 0.09 meV (Figure 4b). The magnetization data (Figure 2b) establish that the ground state is $|S = {}^3/_2\rangle$, and therefore, the cold transitions must be between this level and the first and second excited states, which are $|S = {}^1/_2\rangle$ and $|S = {}^5/_2\rangle$, respectively (Figure 4c). (Note: the spectra show the presence of significant anisotropy; hence, the description of transitions in terms of total $S$ is an approximate but convenient labeling scheme). The hot band then arises from the $|S = {}^1/_2\rangle$ first excited state. The simulation of the INS spectra provides a good determination of the Cr−Cr exchange interaction and fixes this parameter at $J_{CrCr}/k$ = 20 K, in agreement with the magnetization and susceptibility data (Figure 2). The ground-state $S = {}^3/_2$ quartet is split into two doublets by magnetic anisotropy. This splitting is directly detected in compound **1** by the peak at 0.09 meV (Figure 4b). The zero-field splitting parameters $d_i$ and the rhombic parameters $e_i$ were determined from a simultaneous fit of high-resolution INS and EPR spectra (see below), as INS alone does not allow us to distinguish between the contributions of $d_i$ and $e_i$ to the zero-field splitting.

The combination of magnetic and heat capacity measurements, supported by the INS results, allows us to derive the low-energy spectrum for **1** shown in Figure 4c.

*Compound 2: $Cr_7Mn$.* To model the data for **2**, we used the spin Hamiltonian parameters (SHPs) from compound **1** as a starting point, adding parameters to account for the paramagnetic manganese site. As with **1**, the magnetic susceptibility $\chi$ of **2** (Figure S1a in the Supporting Information) increases slowly with decreasing temperature, with a broad maximum

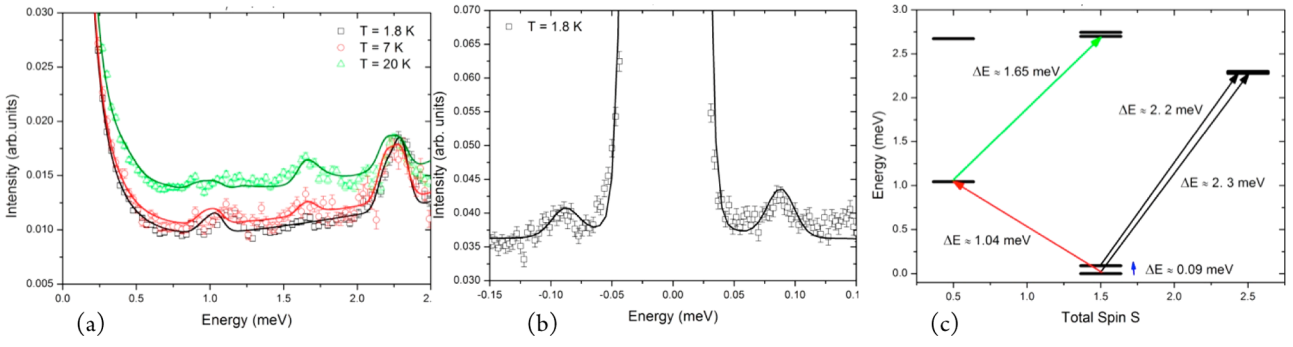


**Figure 4.** INS data for **1**. (a) High-energy transfer spectra from 0 to 2.5 meV at 1.8 K (black squares), 7 K (red circles), and 20 K (green triangles). The solid lines show simulations based on parameters given in Table 1. (b) High-resolution/low-energy spectrum at 1.8 K (black squares) with simulation (solid line). (c) Low-energy spectrum and observed INS transitions for **1**.


dx.doi.org/10.1021/ja5047445 | J. Am. Chem. Soc. 2014, 136, 9763−9772

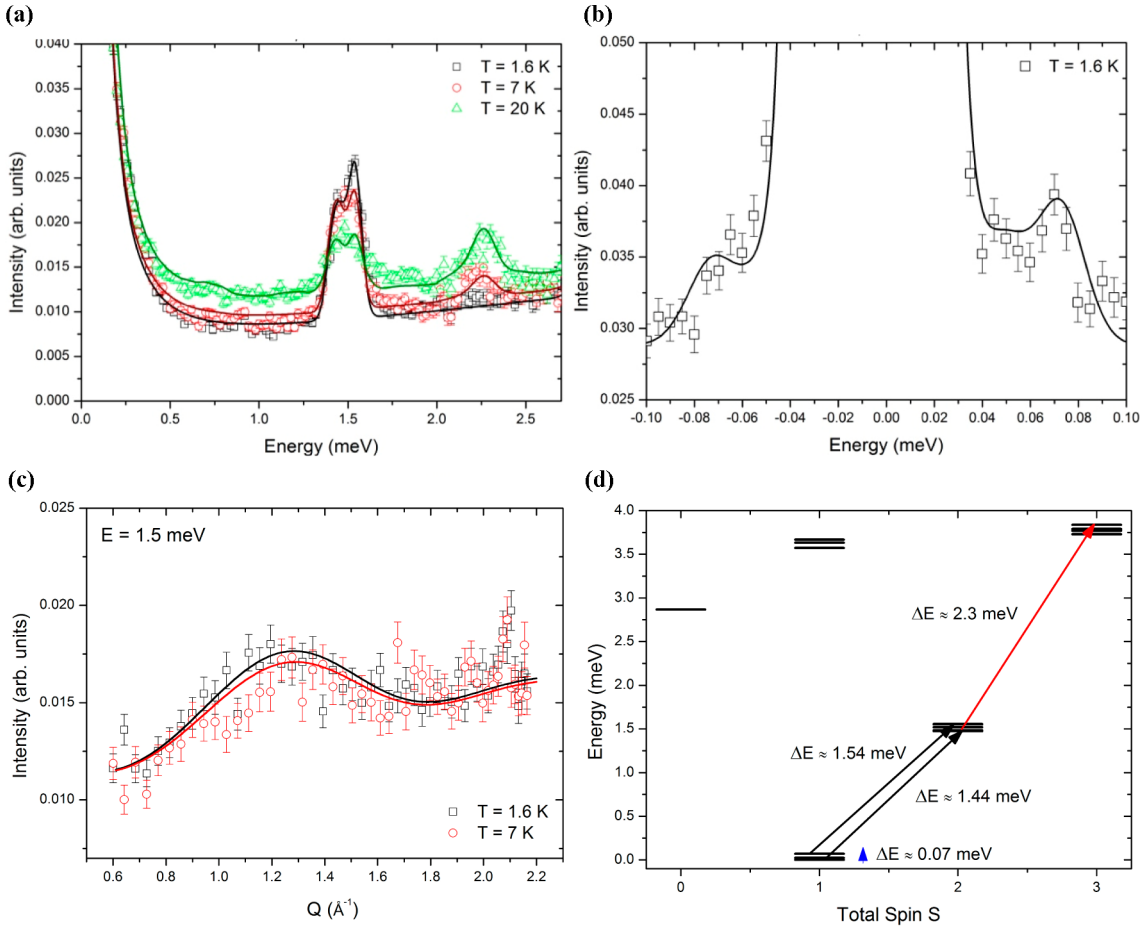


**Figure 5.** INS data for **2**. (a) High-energy transfer spectra from 0 to 2.5 meV at 1.6 K (black squares), 7 K (red circles), and 20 K (green triangles). (b) High-resolution/low-energy spectrum at 1.6 K. The solid lines in (a) and (b) show simulations using parameters in Table 1. (c) $Q$ dependence of the cold peak at $E$ = 1.5 meV appearing in the INS spectra of **2** shown in (a), compared with theoretical simulations (solid lines) at two different temperatures ($T$ = 1.8 and 7 K). (d) Low-energy spectrum and observed INS transitions for **2**.

around 50 K, until 12 K, below which $\chi_m$ rises rapidly. $\chi_m T$ falls with temperature, showing that the interaction between spins is antiferromagnetic. The saturation value of the magnetization at 2 K is 2.0 $\mu_B$ (Figure S1b), showing that there is a ground spin state $|S = 1\rangle$. Fitting the magnetic data with $J_{CrCr}/k$ fixed at 20 K from compound **1** allows us to derive $J_{CrMn}/k$ as 12 K.

Specific heat data confirm the exchange interactions and allow the parameters for the zero-field splitting of the lowest multiplets to be determined. An excellent fit of the data can be obtained considering the lattice contribution with the same Debye parameters of **1**, that is, $\theta_D$ = 156 K and $\varepsilon$ = 0.4 $K^{-1}$ (Figure S2 in the Supporting Information). The zero-field curve (black) shows the Schottky anomaly at the lowest temperature due to the splitting of the ground spin state $|S = 1\rangle$.

INS spectra were measured on powder samples of **2** at 1.6, 7.0, and 20 K and show three cold transitions at 0.07, 1.44, and 1.54 meV and a single hot transition at 2.3 meV (Figure 5a and 5b). The magnetization data show that the ground state is $|S = 1\rangle$; the lowest-energy transition is an intramultiplet transition (Figure 5b) and hence is a direct measure of the zero-field splitting of the ground-state triplet. The other two cold bands are transitions from this state to the first excited state $|S = 2\rangle$, with the splitting due to anisotropy in both the $|S = 1\rangle$ and $|S = 2\rangle$ states (Figure 5a). The hot band is due to a transition from the $|S = 2\rangle$ state to an $|S = 3\rangle$ state. The positions of these transitions match those predicted from the exchange interactions derived from the magnetic and specific heat data. The simulations shown use zero-field splitting parameters $d_{Cr}/k$ = −0.34 K and $e_{Cr}/k$ = −0.09 K (fixed from the EPR study of **1**; see below) and $d_{Mn}/k$ = −0.04 K (from a simultaneous fit of the EPR and INS spectra of **2**; see below). For compound **2**, we also measured the momentum transfer ($Q$), i.e. the modulus of the scattering vector, dependence of the main cold transition at 1.54 meV at 1.6 and 7 K (Figure 5c). The momentum transfer is defined as $Q = \boldsymbol{k} - \boldsymbol{k}'$, where $\boldsymbol{k}'$ and $\boldsymbol{k}$ are the wave vectors of the scattered and incident neutrons. The data show the typical $Q$ dependence of an intermultiplet transition, with an oscillatory behavior related to distances between the metal ions around the ring. These data are well-reproduced by our calculations obtained with the parameters reported in Table 1, thus confirming the assignment of the observed magnetic transitions.

The combination of magnetic and heat capacity measurements, supported by the INS results, allows us to derive the low-energy spectrum for **2** shown in Figure 5d.

*Compound 3: $Cr_7Ni$.* To model the data for compound **3**, we begin with the SHPs used to model the data for **1** and introduce additional parameters to allow for the paramagnetic $Ni^{II}$ ion. The magnetic susceptibility $\chi$ of **3** (Figure S3a in the Supporting Information) increases slowly with decreasing temperature with a well-defined maximum at 40 K, then reaches a minimum value at 12 K before rising rapidly. The


dx.doi.org/10.1021/ja5047445 | J. Am. Chem. Soc. 2014, 136, 9763−9772

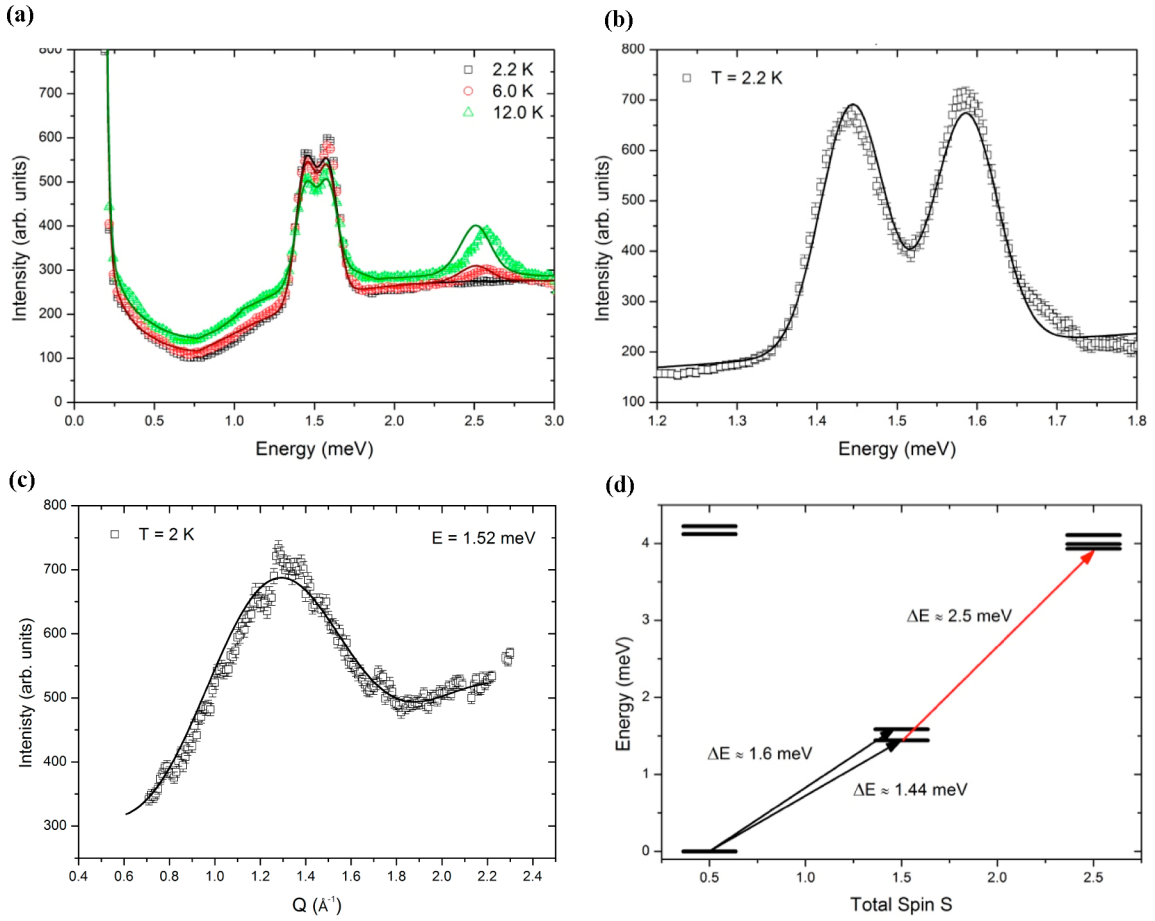


**Figure 6.** INS data for **3**. (a) Spectra for **3** measured with 4.4 Å incident neutrons at 2.2 K (black squares), 6 K (red circles), and 12 K (green triangles). The solid lines show simulations based on the parameters given in Table 1. (b) High-resolution spectrum measured with 5.2 Å incident neutrons at 2.2 K (black squares) with simulation (solid line). (c) $Q$ dependence of the cold peak at $E$ = 1.5 meV appearing in the INS spectra of **3** shown in (a), compared with theoretical estimates (solid lines) at 2 K. (d) Low-energy spectrum and observed INS transitions for **3**.

saturation value of the magnetization at 2 K is close to 1.0 $\mu_B$ (Figure S3b), showing that the ground spin state is $|S = {}^1/_2\rangle$. With the $J_{CrCr}/k$ value found by fitting the data for **1**, the magnetic data for **3** were fitted with $J_{CrNi}/k$ = 30 K.

The specific heat data can also be fitted using the energy gap between the ground $|S = {}^1/_2\rangle$ doublet and the lowest excited states while keeping the same lattice parameters as in **1** and **2** (Figure S4 in the Supporting Information). The zero-field curve shows no Schottky anomaly at the lowest temperature, consistent with the ground state of **3** being an $|S = {}^1/_2\rangle$ spin doublet.

INS spectra were measured at 2.2, 6, and 12 K (Figure 6a). Two cold peaks at 1.44 and 1.6 meV and a hot peak at 2.5 meV are seen. The magnetization data show that the ground state is $|S = {}^1/_2\rangle$, so the two cold peaks are due to transitions to the $|S = {}^3/_2\rangle$ state, with the splitting of these two peaks due to the anisotropy of the $|S = {}^3/_2\rangle$ state. We also investigated these two peaks with higher resolution at 2.2 K in order to better resolve the transitions and to estimate the zero-field splitting of compound **3** (Figure 6b). The hot band at 2.5 meV is from the $|S = {}^3/_2\rangle$ state to the $|S = {}^5/_2\rangle$ state. The INS spectra can be fitted using the $J_{CrCr}/k$ value taken from the fit of **1** and including a single exchange parameter of $J_{CrNi}/k$ = 30 K. The simulations reported in Figure 6 use zero-field splitting parameters $d_{Cr}/k$ = −0.34 K and $e_{Cr}/k$ = −0.09 K (fixed from **1**) along with $d_{Ni}/k$ = −7.3 K and $e_{Ni}/k$ = 0.75 K (from a simultaneous fit of the EPR and INS spectra of **3**; see below). As for compound **2**, we also measured the $Q$ dependence of the main cold transition at 1.52 meV at 2 K. Again the data show the typical $Q$ dependence of an intermultiplet transition and are well-reproduced by our calculations using the parameters in Table 1 (Figure 3c).

The combination of magnetic and heat capacity measurements, supported by the INS results, allows us to derive the low-energy spectrum for **3** shown in Figure 6d.

**Electronic Absorption and EPR Spectroscopy.** The EPR spectra of compounds **1**−**3** are rich with, in each case, contributions from the bottom two spin multiplets. However, before these are discussed it is worth examining the electronic absorption spectra of compounds **1**−**3** and comparing them with the spectra of the previously studied family of green {$Cr_7M$} rings (Figure S5 in the Supporting Information). The spectra are dominated by absorptions due to $Cr^{III}$, regardless of the identity of the divalent metal site. In compounds **1**−**3**, the $^4A_2 \rightarrow {}^4T_2$ transition that defines $\Delta_o$ is found at 17 900 $cm^{-1}$, compared with 16 200 $cm^{-1}$ found in the green rings. This reflects the presence of the stronger-field alkoxide donors in **1**−**3** compared with the fluoride donors in the green rings. A similar change in the electronic absorption spectra was found in moving from $[CrF(O_2C^tBu)_2]_8$ to $[Cr(OH)(O_2C^tBu)_2]_8$.[21] The stronger crystal field for compounds **1**−**3** should lead to less mixing of excited states into the $^4A_2$ ground state, and


dx.doi.org/10.1021/ja5047445 | J. Am. Chem. Soc. 2014, 136, 9763−9772

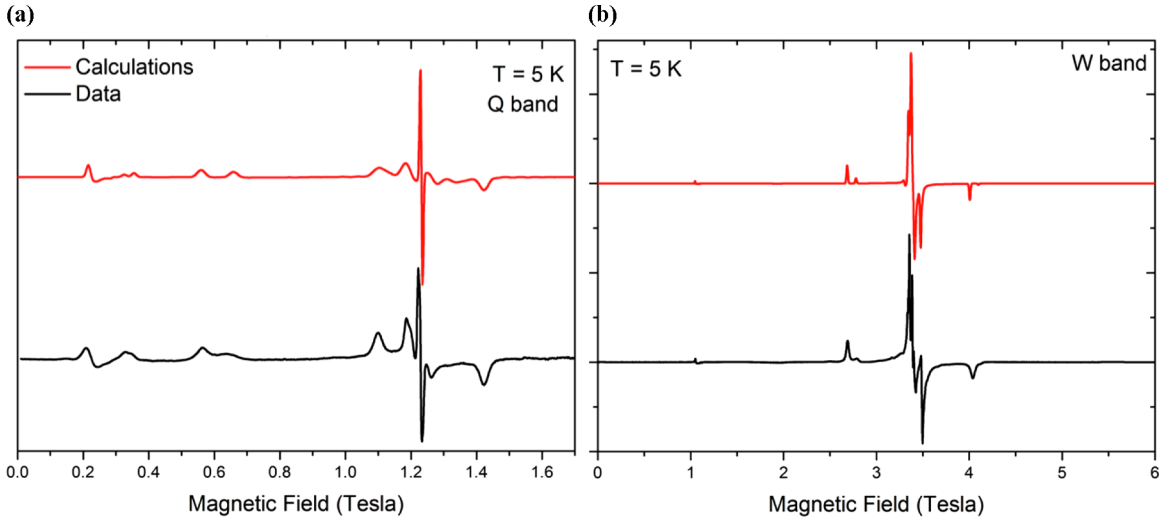


**Figure 7.** (a) Q-band (34.1212 GHz) EPR spectrum of **1** (black) and simulation (red). (b) W-band (94.96804) EPR spectrum of **1** (black) with simulation (red). The spectra were measured on powder samples at 5 K; the simulations are based on the parameters in Table 1.

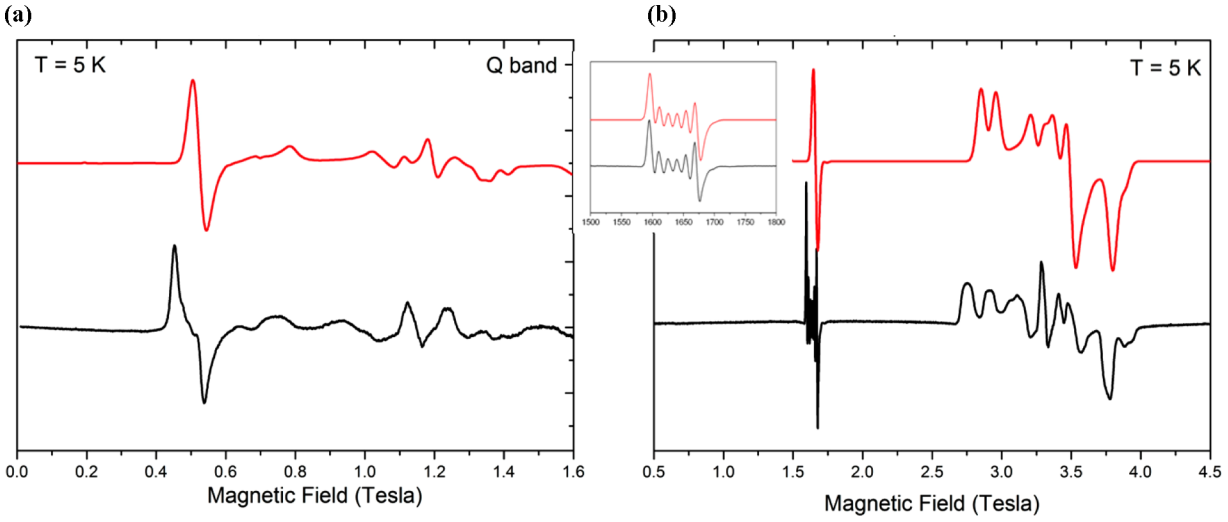


**Figure 8.** (a) Q-band (34.158 GHz) EPR spectrum of **2** (black) with simulation (red). (b) W-band (93.982 GHz) EPR spectrum of **2** (black) with simulation (red). Inset: expansion of the "$\Delta m_s = \pm 2$" transition within the $|S = 1\rangle$ ground state and the simulation as described in the text. The spectra were measured on powder samples at 5 K; the simulations are based on the parameters in Table 1.

hence, we would predict a smaller single-ion anisotropy for the $Cr^{III}$ ions in the purple rings compared with the green rings. It is also noticeable that we cannot resolve features for the several different chromium coordination environments in **1**–**3**.

The Q- and W-band EPR spectra (34 and 94 GHz, respectively) of **1** at 5 K (Figure 7) are dominated by the $|S = {}^3/_2\rangle$ ground state, which give resonances across a broad magnetic field range, and sharper features in the $g = 2$ region that are due to the $|S = {}^1/_2\rangle$ lowest-lying excited state, as assigned by spectrum simulation. Simulation using the microscopic Hamiltonian in eq 1 with $J_{CrCr}$ determined from INS and thermodynamic measurements gives the local zero-field splitting parameters $d_{Cr}/k = -0.34$ and $e_{Cr}/k = -0.09$ K. These parameters were also included in eq 1 to calculate the INS spectra shown in Figure 4. At the W band, the $|S = {}^3/_2\rangle$ spectrum can be analyzed with an effective total spin model to give $D/k = -0.47$ K and $|E/D| = 0.23$ where $D$ and $E$ are the axial and rhombic zero-field splitting parameters that characterize the total-spin ground state, in this case $|S = {}^3/_2\rangle$, in the strong-exchange limit.

The Q- and W-band EPR spectra of **2** at 5 K (Figure 8) are again dominated by the two lowest spin multiplets: a wide-spanning spectrum due to the $|S = 1\rangle$ ground state and transitions near $g = 2$ due to the $|S = 2\rangle$ first excited state. These can be simulated using the exchange parameters found from the INS data and the Cr zero-field splitting parameters determined from simulations of **1**, leaving only two free parameters describing the local zero-field splitting for $Mn^{II}$ to simulate these complex spectra. Simultaneous simulation of the Q- and W-band EPR spectra and the INS spectra gave $d_{Mn}/k = -0.04$ K, and we found no requirement to include a rhombic $e_{Mn}$ term. As for compound **1**, we can also determine the effective zero-field splitting parameters of the $|S = 1\rangle$ total-spin ground state; these are $D/k = -0.79$ K and $|E/D| = 0.16$. The lowest-field features in the Q- and W-band spectra (at ca. 0.5 and 1.6 T, respectively) are due to the formally spin-forbidden $\Delta m_s = \pm 2$ transition within this multiplet. These features are sharper because, describing them in terms of an isolated $|S = 1\rangle$ state, such transitions are unaffected by $D$ strain.[16b] The line widths are sufficiently small that the $^{55}Mn$ ($I = {}^5/_2$) hyperfine features


dx.doi.org/10.1021/ja5047445 | J. Am. Chem. Soc. 2014, 136, 9763–9772

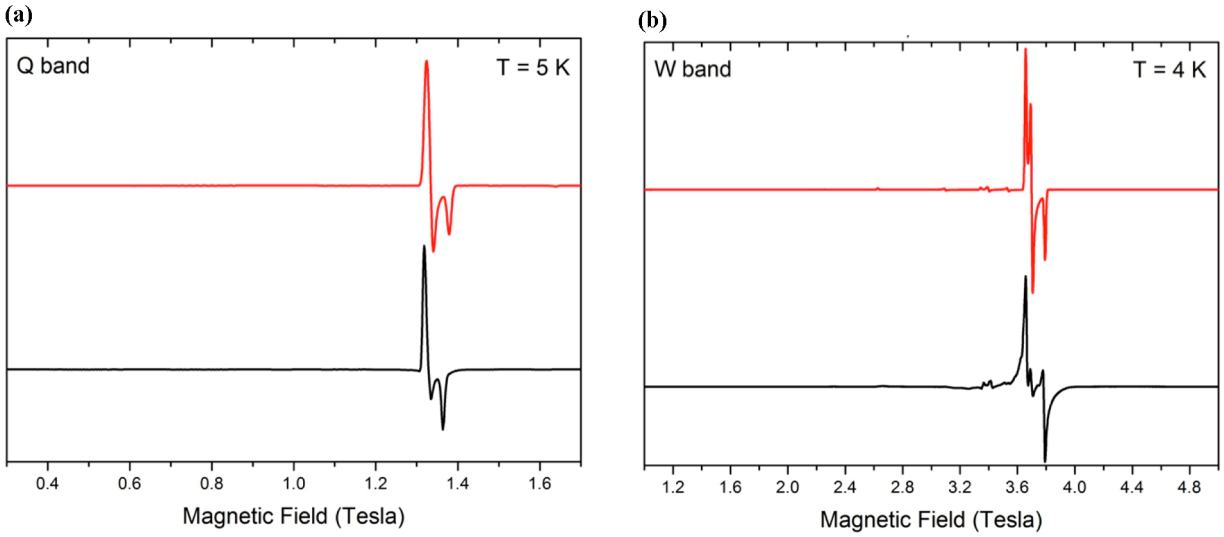


**Figure 9.** (a) Q-band (34.1587 GHz) EPR spectrum of **3** (black) with simulation (red). (b) W-band (93.90816 GHz) EPR spectrum of **3** (black) with simulation (red). The spectra were measured on powder samples at 5 K; the simulations are based on parameters in Table 1.

are resolved: these can be simulated with $A = 134 \times 10^{-4}$ cm$^{-1}$ for $|S = 1\rangle$ (Figure 8 inset). It should be noted that this is the projection of the single-ion ($s = {}^5/_2$) Mn hyperfine interaction [with typical values of $(80-100) \times 10^{-4}$ cm$^{-1}$] onto the $|S = 1\rangle$ total-spin ground state and is much larger than the "true" hyperfine interaction as a consequence of the antiferromagnetic $J_{CrMn}$ interaction.

The Q-band EPR spectrum of **3** at 5 K (Figure 9a) is relatively simple, showing a sharp anisotropic set of $g$ values centered at 1.32 T due to the $|S = {}^1/_2\rangle$ ground state. The W-band spectrum (Figure 9b) is more complicated since the $|S = {}^3/_2\rangle$ first excited state is now significantly populated because the larger applied fields stabilize the $m_s = -{}^3/_2$ component relative to the $|S = {}^1/_2\rangle$ ground state. The near-axial $g$ values for the ground state are easily reproduced via the Hamiltonian in eq 1 by the anisotropic $g$ values of the Ni$^{II}$ ion: $g_{xx}^{Ni} = g_{yy}^{Ni} = 2.18$, $g_{zz}^{Ni} = 2.25$. With the parameters found from simulations of **1**, simultaneous fitting of the Q- and W-band EPR spectra and the INS spectra gave $d_{Ni}/k = -7.3$ K and $e_{Ni}/k = 0.75$ K. The signs of $d_{Ni}$ and $e_{Ni}/e_{Cr}$ were determined unambiguously by fitting of the EPR spectra, and $d_{Ni}$ is consistent with the sense of Ni $g$ anisotropy ($g_{xx}^{Ni} = g_{yy}^{Ni} < g_{zz}^{Ni}$). These parameters are consistent with those determined by thermodynamic measurements.

**Analysis.** We have probed three isostructural heterometallic rings by a large array of experimental techniques and fitted the data obtained using an approach based on a microscopic Hamiltonian. The set of SHPs is summarized in Table 1. To obtain these SHPs, we made significant assumptions.

First, to fit the magnetic and heat capacity data for **1**, we assumed that a single $J_{CrCr}$ interaction could be used, despite the presence of six crystallographically distinct Cr···Cr interactions within the heterometallic ring. This assumption also allows us to interpret the INS data. It is not immediately obvious that this should work; previously we have found that INS data require more exchange interactions in open-chain {Cr$_6$} horseshoes, even where the magnetic data can be fitted with a single exchange interaction.[22] Second, we interpreted these data and the EPR spectra with the assumption of a single $d_{Cr}$ parameter and a single $e_{Cr}$ parameter when crystallographically there are seven unique Cr$^{III}$ sites among which there are four distinct coordination environments. Third, the microscopic Hamiltonian approach requires an assumption about the projection of the single-ion anisotropy parameters onto the cluster anisotropy; we have assumed that the principal axes are all coparallel. In our previous studies of the green {Cr$_7$M} rings, there was a fourfold rotation axis perpendicular to the plane of the ring, and we could assume that the single-ion $z$ axes were parallel to this fourfold axis. Here there is no symmetry, but we have had to make the same assumption about the local axes and the anisotropy axis of the ring.

To interpret the data for **2** and **3**, we made the further assumptions that the SHPs derived from **1** are not modified upon moving to these other compounds. This seems to be a reasonable assumption. We also made the assumption that there is only a single $J_{CrM}$ interaction, despite the presence of three bridges on one edge and two on the other and the two different bridging angles (ca. 122 and 131°; see above). This is a very different structural case compared with the green {Cr$_7$M} rings, where every edge is chemically identical; even there, for a {Cr$_7$Cu} ring we found that the INS data clearly differentiated two $J_{CrCu}$ interactions.[23] The major difference there is the very anisotropic electronic structure of a Cu$^{II}$ ion, in which the $z$ axis is very different from the $xy$ plane. The observation here is that the minimal model with only one $J_{CrM}$ interaction works, and we have no justification in adding an additional parameter. The large 131° angle may explain why $J_{CrNi}$ is more antiferromagnetic in **3** compared with the green {Cr$_7$Ni} ring (see Table 2). We then included a $d_{Mn}$ parameter for **2** and a large $d_{Ni}$ and $e_{Ni}$ for **3**. Again the implicit assumption is that the anisotropy axes for the divalent ions are coparallel with those of the Cr$^{III}$ sites.

The inescapable conclusion therefore is that parameters are remarkably transferable between structures but also between chemically distinct positions in the same structure. Care has to be taken in introducing more parameters to model data.

**Comparison with the Green {Cr$_7$M} Rings.** We previously studied the compounds [$H_2NMe_2$][$Cr_7MF_8$($O_2C^tBu$)$_{16}$] [M = Zn (**4**), Mn (**5**), Ni (**6**)], where each edge of a regular octagon is bridged by a single fluoride and two pivalate groups. The dominant interaction in both families of compounds is the nearest-neighbor isotropic exchange coupling. The $J_{CrCr}$ values are larger for **1**–**3** than for **4**–**6**


dx.doi.org/10.1021/ja5047445 | J. Am. Chem. Soc. 2014, 136, 9763–9772

(see Tables 1 and 2), pointing to a stronger exchange pathway through bridging alkoxide groups compared with bridging fluoride ions. The exchange interactions were analyzed previously by density functional theory.[26] As far as the anisotropic part of the Hamiltonian is concerned, the zero-field splitting parameters of compounds **4**–**6** were determined from previous INS measurements[24] by the same model used for **1**–**3** and are reported in Table 2. Because of the different symmetries of the two families of compounds, we limit the comparison to the dominant axial contributions (the first term in eq 2). $d_{Cr}$ is smaller in the purple rings than in the green analogues, reflecting the difference in electronic absorption spectra discussed previously (Figure S5 in the Supporting Information). In addition, we found a larger value of $d_{Mn}$ in **5** with respect to **2** and a larger value of $d_{Ni}$ in the purple variant. These differences could be exploited to distinguish spectrally the two kind of molecules in envisaged supramolecular purple–green complexes, which are interesting for implementing quantum information processing and for investigating entanglement in supramolecular systems.

**Table 2. Spin Hamiltonian Parameters for Compounds 4–6 Based on Previous Studies[24]**

| compound | $J_{CrCr}/k$ (K) | $J_{CrM}/k$ (K) | $d_{Cr}/k$ (K) | $d_M/k$ (K) |
|---|---|---|---|---|
| **4** | 16.9 | – | −0.45 | – |
| **5** | 16.9 | 15.9 | −0.45 | −0.13 |
| **6** | 16.9 | 19.6 | −0.45 | −4.6 |

It is worth noting that the EPR spectra of **1**–**3** have narrower line widths than their equivalents in the **4**–**6** family. This is especially noticeable in the resolved hyperfine coupling to Mn in compound **2**. The most likely explanation for the narrower line widths in these powder spectra is that the divalent metal site is ordered in **1**–**3** and disordered in **4**–**6**. A second possible explanation is the decrease in the number of fluoride ligands found in **1**–**3**, with a reduction in unresolved hyperfine coupling to the F nuclei.

## CONCLUSIONS

A broad set of experimental techniques has been used to characterize the physical properties of a series of "purple" {$Cr_7M$} molecular rings, compounds **1**–**3**. This has allowed us to compare directly the magnetic features of these derivatives with same microscopic parameters previously found for the "green" {$Cr_7M$} rings, compounds **4**–**6**. Compounds **1**–**3** have the same structure of the energy spectrum as shown by **4**–**6**. The same ground state is found, depending on the divalent metal included, and the states with the minimal energy for each $S$ value form a parabolic band that closely follows the Landé interval rule (Figure 10).[5,25] We had expected to need a model that contained different exchange interactions, at least for the two differing Cr···M edges. Such a model is computationally feasible but still would involve the fitting of a large number of free parameters. However, the global approach operates on the underlying assumption that structural information is sufficient for the deduction of exchange parameters to model magnetic

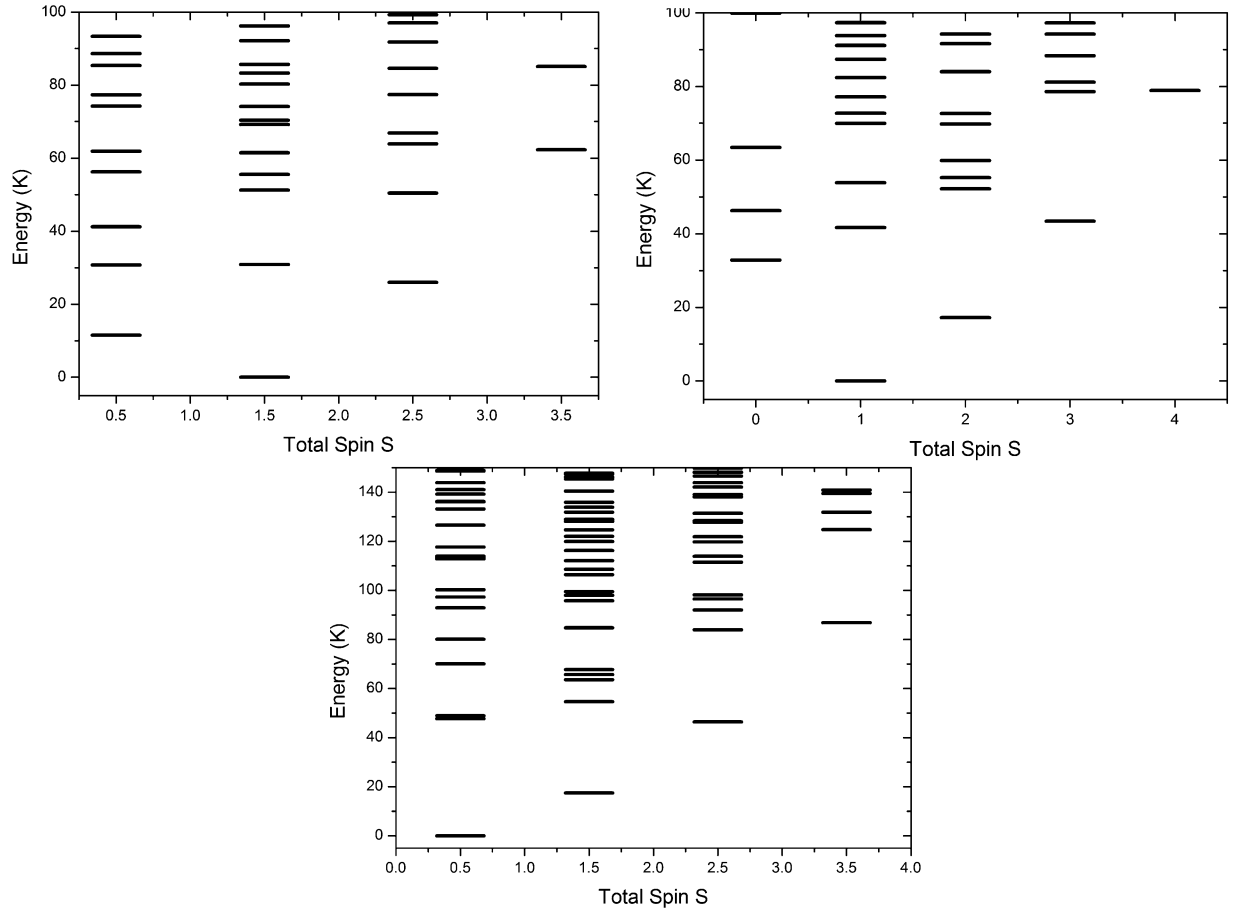


**Figure 10.** Low-energy region of the energy spectrum for compounds **1**–**3**.


dx.doi.org/10.1021/ja5047445 | J. Am. Chem. Soc. 2014, 136, 9763–9772

data. A significant result from this work is that this assumption is not necessary. Our model begins with the experimental data from four different physical methods and uses only the fewest number of parameters required to model all of these experimental data. We have indeed shown that with only two exchange parameters, one $J_{CrCr}$ and one $J_{CrM}$, we can accurately model the bulk magnetization data, neutron scattering spectra, EPR spectra at multiple frequencies, and specific heat data of these highly asymmetric systems. It is not necessary to build models of polymetallic compounds from a belief in magneto-structural correlations; additional spin Hamiltonian parameters should only be introduced when experimental data justify it.

## ■ ASSOCIATED CONTENT

### Supporting Information

Full synthetic and crystallographic details (CIF) and details of the experimental and theoretical procedures used. This material is available free of charge via the Internet at http://pubs.acs.org.

## ■ AUTHOR INFORMATION


### Corresponding Author

richard.winpenny@manchester.ac.uk

### Present Address

[¶]Istituto de Ciencia de Materiales de Aragón, CSIC-Universidad de Zaragoza, Departamento de Física de la Materia Condensada, 50009 Zaragoza, Spain.


### Notes

The authors declare no competing financial interest.

## ■ ACKNOWLEDGMENTS

We thank the EPSRC (UK) for funding for the National EPR Facility and Service, for a postdoctoral position (to G.A.T., Grant EPSRC EP/J009377/1), for the Centre for Doctoral Training "NoWNANO", and for funding for X-ray equipment (EP/K039547/1). We thank ILL for funding for a studentship (to M.L.B.) and ILL and ISIS for providing beamtime. This work was financially supported by the Italian FIRB Project RBFR12RPD1 of the Italian MIUR "New Challenges in Molecular Nanomagnetism: From Spin Dynamics to Quantum-Information Processing."

## ■ REFERENCES


(1) Gatteschi, D.; Sessoli, R.; Villain, J. *Molecular Nanomagnets*; Oxford University Press: Oxford, U.K., 2006.

(2) Thomas, L.; Lionti, F.; Ballou, R.; Gatteschi, D.; Sessoli, R.; Barbara, B. *Nature* **1996**, *383*, 145.

(3) Wernsdorfer, W.; Sessoli, R. *Science* **1999**, *284*, 133.

(4) Caneschi, A.; Gatteschi, D.; Laugier, J.; Rey, P.; Sessoli, R.; Zanchini, C. *J. Am. Chem. Soc.* **1988**, *110*, 2795.

(5) Taft, K. L.; Delfs, C. D.; Papaefthymiou, G. C.; Foner, S.; Gatteschi, D.; Lippard, S. J. *J. Am. Chem. Soc.* **1994**, *116*, 823.

(6) Waldmann, O.; Stamatatos, T. C.; Christou, G.; Güdel, H. U.; Sheikin, I.; Mutka, H. *Phys. Rev. Lett.* **2009**, *102*, No. 157202.

(7) Baker, M. L.; Guidi, T.; Carretta, S.; Mutka, H.; Timco, G.; McInnes, E. J. L.; Amoretti, G.; Winpenny, R. E. P.; Santini, P. *Nat. Phys.* **2012**, *8*, 906.

(8) Baker, M. L.; Timco, G. A.; Piligkos, S.; Mathieson, J.; Mutka, H.; Tuna, F.; Kozłowski, P.; Antkowiak, M.; Guidi, T.; Gupta, T.; Rath, H.; Woolfson, R. J.; Kamieniarz, G.; Pritchard, R. G.; Weihe, H.; Cronin, L.; Rajaraman, G.; Collison, D.; McInnes, E. J. L.; Winpenny, R. E. P. *Proc. Natl. Acad. Sci. U.S.A.* **2012**, *109*, 19113.

(9) (a) Laye, R. H.; Larsen, F. K.; Overgaard, J.; Muryn, C. A.; McInnes, E. J. L.; Rentschler, E.; Sanchez, V.; Teat, S. J.; Güdel, H. U.; Waldmann, O.; Timco, G. A.; Winpenny, R. E. P. *Chem. Commun.* **2005**, 1125. (b) Timco, G. A.; McInnes, E. J. L.; Winpenny, R. E. P. *Chem. Soc. Rev.* **2013**, *42*, 1796.

(10) Carretta, S.; Santini, P.; Amoretti, G.; Affronte, M.; Ghirri, A.; Sheikin, I.; Piligkos, S.; Timco, G. A.; Winpenny, R. E. P. *Phys. Rev. B* **2005**, *72*, 060403.

(11) Carretta, S.; Santini, P.; Amoretti, G.; Guidi, T.; Copley, J. R. D.; Qiu, Y.; Caciuffo, R.; Timco, G.; Winpenny, R. E. P. *Phys. Rev. Lett.* **2007**, *98*, No. 167401.

(12) (a) Ardavan, A.; Rival, O.; Morton, J. J. L.; Blundell, S. J.; Tyryshkin, A. M.; Timco, G. A.; Winpenny, R. E. P. *Phys. Rev. Lett.* **2007**, *98*, No. 057201. (b) Wedge, C. J.; Timco, G. A.; Spielberg, E. T.; George, R. E.; Tuna, F.; Rigby, S.; McInnes, E. J. L.; Winpenny, R. E. P.; Blundell, S. J.; Ardavan, A. *Phys. Rev. Lett.* **2012**, *108*, No. 107204.

(13) (a) Troiani, F.; Ghirri, A.; Affronte, M.; Carretta, S.; Santini, P.; Amoretti, G.; Piligkos, S.; Timco, G.; Winpenny, R. E. P. *Phys. Rev. Lett.* **2005**, *94*, No. 207208. (b) Santini, P.; Carretta, S.; Troiani, F.; Amoretti, G. *Phys. Rev. Lett.* **2011**, *107*, No. 230502.

(14) Timco, G. A.; Carretta, S.; Troiani, F.; Tuna, F.; Pritchard, R. G.; McInnes, E. J. L.; Ghirri, A.; Candini, A.; Santini, P.; Amoretti, G.; Affronte, M.; Winpenny, R. E. P. *Nat. Nanotechnol.* **2009**, *4*, 173.

(15) Moro, F.; Kaminski, D.; Tuna, F.; Whitehead, G. F. S.; Timco, G. A.; Collison, D.; Winpenny, R. E. P.; Ardavan, A.; McInnes, E. J. L. *Chem. Commun.* **2014**, *50*, 90.

(16) (a) Piligkos, S.; Bill, E.; Collison, D.; McInnes, E. J. L.; Timco, G. A.; Weihe, H.; Winpenny, R. E. P.; Neese, F. *J. Am. Chem. Soc.* **2007**, *129*, 760. (b) Piligkos, S.; Weihe, H.; Bill, E.; Neese, F.; El Mkami, H.; Smith, G. M.; Collison, D.; Rajaraman, G.; Timco, G. A.; Winpenny, R. E. P.; McInnes, E. J. L. *Chem.—Eur. J.* **2009**, *15*, 3152.

(17) Timco, G. A.; McInnes, E. J. L.; Pritchard, R. G.; Tuna, F.; Winpenny, R. E. P. *Angew. Chem., Int. Ed.* **2008**, *47*, 9681.

(18) Saalfrank, R. W.; Bernt, I.; Uller, E.; Hampel, F. *Angew. Chem., Int. Ed. Engl.* **1997**, *36*, 2482.

(19) (a) Hegetschweiler, K.; Smalle, H.; Streit, H. M.; Schneider, W. *Inorg. Chem.* **1990**, *29*, 3625. (b) Shaw, R.; Tidmarsh, I. S.; Laye, R. H.; Breeze, B.; Helliwell, M.; Brechin, E. K.; Heath, S. L.; Murrie, M.; Ochsenbein, S.; Güdel, H.-U.; McInnes, E. J. L. *Chem. Commun.* **2004**, 1418. (c) Brechin, E. K. *Chem. Commun.* **2005**, 5141. (d) Langley, S. K.; Moubaraki, B.; Forsyth, C. M.; Gass, I. A.; Murray, K. S. *Dalton Trans.* **2010**, *39*, 1705. (e) Langley, S. K.; Moubaraki, B.; Murray, K. S. *Dalton Trans.* **2010**, *39*, 5066. (f) Schmidt, S.; Prodius, D.; Mereacre, V.; Kostakis, G. E.; Powell, A. K. *Chem. Commun.* **2013**, *49*, 1696. (g) Abbas, G.; Kostakis, G. E.; Lan, Y. H.; Powell, A. K. *Polyhedron* **2012**, *41*, 1.

(20) Borrás-Almenar, J. J.; Clemente-Juan, J. M.; Coronado, E.; Tsukerblat, B. S. *Inorg. Chem.* **1999**, *38*, 6081.

(21) Christian, P.; Rajaraman, G.; Harrison, A.; McDouall, J. J. W.; Raftery, J. T.; Winpenny, R. E. P. *Dalton Trans.* **2004**, 1511.

(22) Baker, M. L.; Bianchi, A.; Carretta, S.; Collison, D.; Docherty, R.; McInnes, E. J. L.; McRobbie, A.; Muryn, C. A.; Mutka, H.; Piligkos, S.; Rancan, M.; Santini, P.; Timco, G. A.; Tregenna-Piggott, P. L. W.; Tuna, F.; Güdel, H. U.; Winpenny, R. E. P. *Dalton Trans.* **2011**, *40*, 2725.

(23) Baker, M. L.; Piligkos, S.; Bianchi, A.; Carretta, S.; Collison, D.; McDouall, J. J. W.; McInnes, E. J. L.; Mutka, H.; Timco, G. A.; Tuna, F.; Vadivelu, P.; Weihe, H.; Güdel, H. U.; Winpenny, R. E. P. *Dalton Trans.* **2011**, *40*, 8533.

(24) Caciuffo, R.; Guidi, T.; Amoretti, G.; Carretta, S.; Santini, P.; Mondelli, C.; Timco, G.; Muryn, C. A.; Winpenny, R. E. P. *Phys. Rev. B* **2005**, *71*, No. 174407.

(25) Schnack, J.; Luban, M. *Phys. Rev. B* **2001**, *63*, No. 014418.

(26) (a) Bellini, V.; Affronte, M. *J. Phys. Chem. B* **2010**, *114*, 14797. (b) Chiesa, A.; Carretta, S.; Santini, P.; Amoretti, G.; Pavarini, E. *Phys. Rev. Lett.* **2013**, *110*, 157204.